IOP Conference Series: Earth and Environmental Science

Evaluation of the jet distortion by sediment erosion in the needle in the Pelton turbines

To cite this article: Jim Abregu *et al* 2024 *IOP Conf. Ser.: Earth Environ. Sci.* **1385** 012005

Evaluation of the jet distortion by sediment erosion in the needle in the Pelton turbines

Jim Abregu[1], Jonas Scheuer[2], Sajan Satyal[4], Bjørn W. Solemslie[1,3] and Ole G. Dahlhaug[1]

[1] Waterpower Laboratory, Department of Energy & Process Engineering, Norwegian University of Science and Technology, NO-7491, Trondheim, Norway
[2] RWTH Aachen University, Templergraben 55, 52062 Aachen, Germany
[3] Department of Aquatic Biodiversity, Norwegian Institute for Nature Research, NO-7485, Trondheim, Norway
[4] Testing Turbine Laboratory, Kathmandu University, 6250 Dhulikhel, Nepal

E-mail: jim.abregu@ntnu.no

Abstract. In order to succeed in the transition to a more renewable energy sector, the hydropower industry must overcome multiple challenges in the coming decades, including the need for faster and reversible turbines to support emerging renewable energy sources. In addition, the location of new projects in tropical and semi-tropical areas poses unique considerations, as does the increase in sediment.

Evaluating sediment erosion in turbines is a critical challenge, which may partly be addressed by analyzing the behavior of water jets from eroded nozzles in Pelton turbines. This paper presents an evaluation of the quality of the jet under various hydraulic conditions, focusing on needle erosion. The study is part of a research project conducted in the Waterpower Laboratory at NTNU, focusing on Pelton turbines.

Furthermore, this paper investigates erosion patterns caused by sediments on the needle and explores the impact on jet performance. Through high-speed visualization and image processing, the behavior of a jet from the needle tip to a representative distance downstream has been investigated. The investigation revealed discernible differences between jets with eroded and uneroded needles in size and edge variation.

1. Introduction

The most significant challenges in hydropower plants exposed to sediment erosion lie in assessing the condition of mechanical components and quantifying the efficiency losses across all their components. Primarily, the nozzle and runner components experience the highest erosion levels. However, most metallic elements in contact with sediment-laden water within a hydropower plant also incur efficiency losses[1]. The extent of erosion these components are subject to correlates with the angle and velocity to the component surface[2] as is shown in Figure 1.

This study specifically examines needle erosion, without considering the impact on the jet profile from other eroded turbine components, such as the outlet seat ring of the nozzle Figure 1(a).

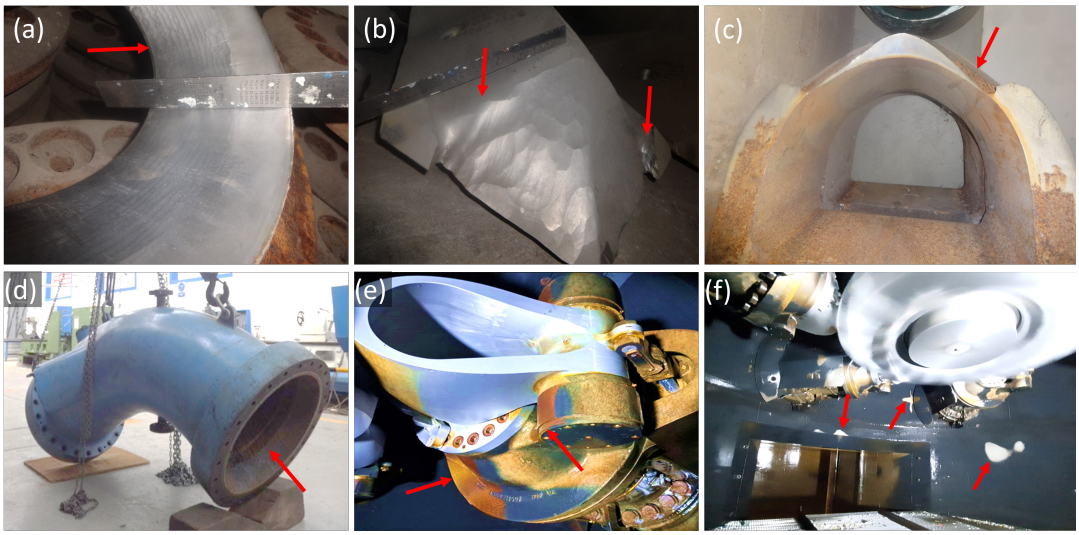

Figure 1: (a)Erosion on seat ring in the outlet part of the nozzle, HPP at Ancash, Peru. (b) Erosion on needle shields, HPP at Ancash, Peru. (c) Erosion on deflectors, HPP at Ancash, Peru. (d) Erosion and pipes, HPP at Ancash, Peru. (e) Erosion on nozzle outlet, HPP at Junín, Peru. (f) Erosion on turbine chamber, HPP at Junín, Peru.

2. Erosion on needles

The erosion behavior of needles varies based on the hydraulic conditions within the power plant and the specific characteristics of the sediments. However, a significant distinction arises when the needles are coated with tungsten carbide due to the material's exceptional hardness and inherent fragility as shown in Figure 2. Certainly, the erosion-induced material loss in the needle leads to varying angles within the jet profile, significantly impacting the overall performance of the jet[3]. This research is mainly focused on erosion over the uncoated surface of a Pelton needle.

Figure 2: Stages of erosion on a coated needle, HPP at Ancash, Peru.

2.1. Types of erosion on uncoated needles

Insufficient instrumentation or the inadequacy of existing instrumentation for monitoring sediment influx can lead to episodes of accelerated erosion over short intervals as shown in Figure 3(c). The scope of this research is specifically centered around normal erosion processes that occur over longer periods, allowing for analysis and prediction of their consequences.

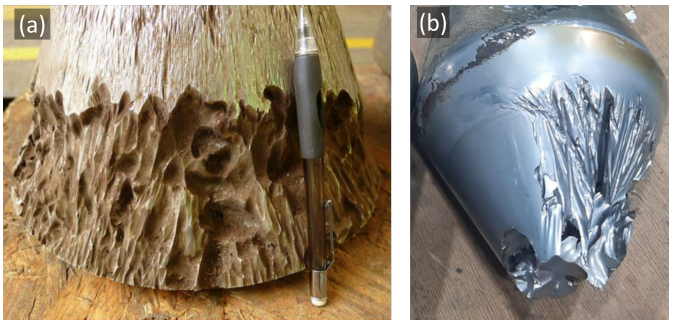

Figure 3: High erosion due to high sediment concentration during short periods (a)Uncoated needle[4]. (b)Uncoated needle during El Niño phenomena, HPP at Ancash, Peru.

The erosion of needles primarily begins with abrasion, resulting in the formation of ripples or wave patterns on the surface[5]. The characteristics of these patterns depend on the velocity of water and sediment conditions. Over time, these wave patterns tend to elongate and deepen as shown in Figure 4, influenced by the sediment conditions.

Within the needle and the seat ring in the nozzle, erosion exhibits spatial variability, resulting in distinct classifications for various zones[6]. However, accurately predicting the geometry and evolution of these erosion patterns remains a formidable challenge due to the intricate interplay of hydraulics, sediment, and operational factors.

For this study, we employed the initial conditions of a hydropower plant located in Ancash, Peru. The erosion phenomenon observed was replicated, scaled, and applied to the needle geometry of the Pelton turbine test rig located in the Waterpower Laboratory at NTNU. The purpose of evaluating this model was to identify an approach that may be applied to most power plants experiencing typical erosion conditions. In assessing the shape of this erosion, they were approximated to be part of an ellipse with different radios in axial and longitudinal to the line flow, aligning with the measurements given by Ancash's hydropower plant. The geometry of the erosion was standardized to ensure control over both size and shape. Three erosion stages were tested, with and without eroded surface at the same area reduced needle geometry as we see in Figure 5 and Figure 6. This approach allows us to distinguish between the effects of erosion

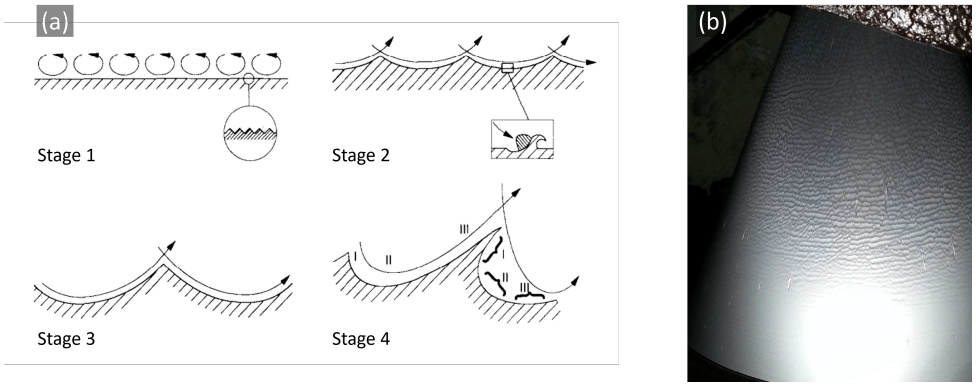

Figure 4: Erosion in the uncoated needle (a)Ripple formation process[5] (b)Erosion patterns on the needle in Hpp at Junin, Peru

and those stemming from the less affected area on the jet behavior. Detailed information can be found Figure 15 in the Appendix.

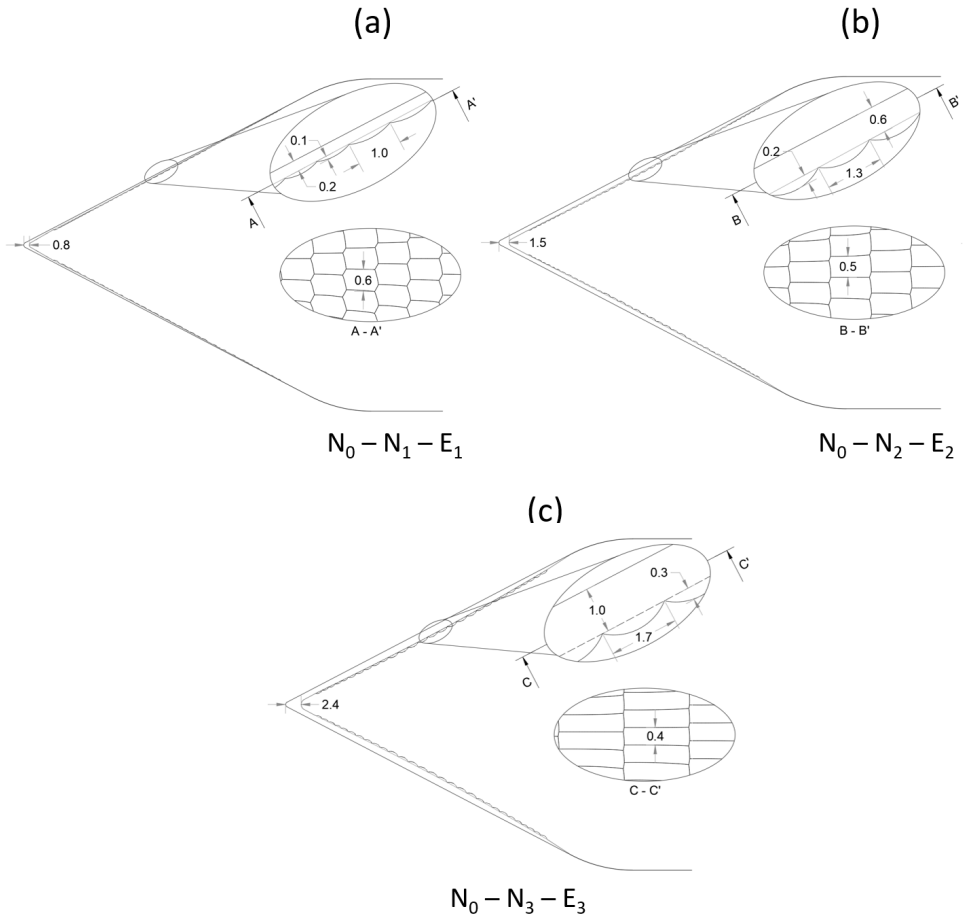

Figure 5: Model erosion used for the experiment. (a) erosion and area reduced model 1 (b) erosion and area reduced model 2 (c) erosion and area reduced model 3

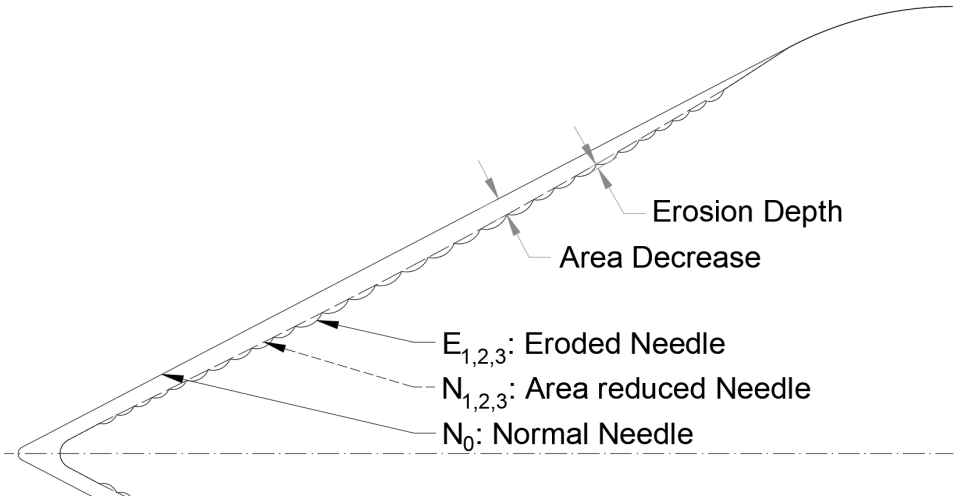

Figure 6: The figure shows a sketch of the main parametric variations between the eroded and uneroded needles.

Needle Type	**Area Decrease (mm)**	**Erosion Depth (mm)**
N_1	0,2	0
E_1	0,2	0,1
N_2	0,6	0
E_2	0,6	0,2
N_3	1,0	0
N_3	1,0	0,3
N_0	0	0

Table 1: Principal parameters for each needle.

The production of the needle involved numerous iterations in order to achieve optimal resolution. After experimenting with various materials and processes, acceptable tolerances were found through resin 3D printing. The printer used was the Sonic Mega 8K, with a theoretical resolution of 28µm. The resin selected was the eSUN Resin Hard-Tough with a surface hardness of 75-81 Shore D.

3. Image Processing and Experimental Setup

The testing was conducted following the IEC standard[7] for calibrations. Each test duration was carefully determined to reduce uncertainty and stabilize hydraulic conditions.

3.1. Image Processing

To distinguish the edges of the water jet, it is important to create a contrast in brightness between the water surface and the background. To achieve this, a white metal plate was positioned below the jet and they were both illuminated by an 110000 lumen bright light, resulting in good, diffused light. This brightness is needed, to capture sharp images at a required shutter speed of 1/40000 seconds. This ensured that the lens received sufficient light to render the jet visible in the frames. Precisely illuminating only the plate, rather than the jet, played an important role in achieving a distinct boundary between the bright background and the dark water jet as is shown in Figure 7. Filming one side at a time, instead of both jet sides simultaneously, prevented the jet itself from appearing bright, maintaining accurate edge detection through the average statistic analysis.

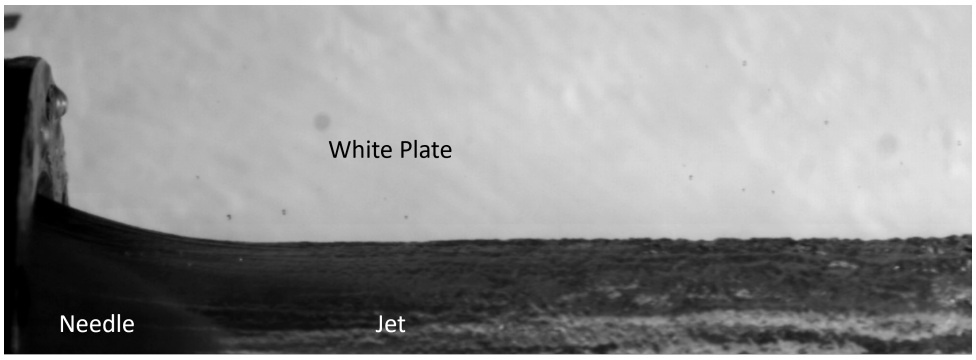

Figure 7: Camera image captured at a shutter speed of 1/400000 seconds to delineate the jet's border along the flow direction

For video frame analysis, the algorithm initially equalizes frames using a calibration matrix. Since the jet's edge is nearly horizontal, with the most significant brightness change occurring along the vertical axis, the algorithm computes pixel gradients along the columns of each frame. The consistent brightness of the plate ensures a low first derivative along the homogeneous white plate until it detects a rapid brightness change at the jet's edge. Subsequently, a threshold is applied to the frame's first derivative, creating a mask where pixels above a certain value appear white (255), while the rest gets black (0). To mitigate frame noise caused by water droplets or local light variations, additional mask groups connected white pixels into objects, turning them black if they exceeded a specific threshold. The program scans all columns from the image's outer edge to detect the first white pixel, storing these pixels in a data frame to create the recognized edge. This process is repeated for 800 images, while 125 frames per second are taken into consideration, which leads to statistical insights of the surface edge behavior of 6.4 seconds.

To ensure metric accuracy, camera calibration is vital. The camera's intrinsic parameters (including focal length, principal point, and axis tilt) and extrinsic parameters (rotation and translation) were obtained by calibrating them with a squared template. The calibration matrix, derived from six images of the template, corrected tangential and radial distortion using the OpenCV library in a Python-based program. Additionally, the calibration established the correlation between focus height metrics and image pixels, resulting in an average value of 0.15 mm per pixel. This conversion enables the presentation of image process statistics on a metric scale.

The setup utilized a Photron FastCam SA5, with a resolution of 1024x1024, to capture top-view images of the jet. A 105 mm lens was attached to the camera to achieve a field of view capturing 140 mm of the jet when measured from the needle tip. To create a well-lit background beneath the jet, an 110000 lumen bright HMI Fresnel lamp was positioned as illustrated in the setup figure 8, illuminating the jet and a white plate positioned below.

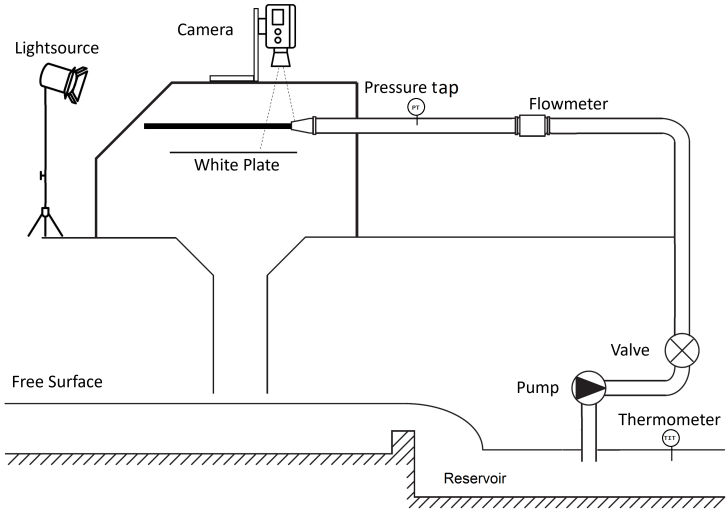

Figure 8: Hydraulic system and camera setup for the jet diameter [8].

Additionally, both inlet pressure and flow rate were measured with a sampling rate of 1000Hz. To comprehensively analyze the variations due to erosion, maintaining a constant net head and flow rate is essential. The requirements for a measurement to be deemed valid can be found below.

Pressure Sensor:

(a) Exhibited a systematic error of $\pm 0.0125\%$ at an average pressure of 3 bars.

Flow Meter:

(a) After calibration, the systematic error of the flow meter was found to be approximately $\pm 0.385\%$.

Total Accuracy Considerations:

(a) To achieve the total accuracy of the net head and volume flow, we must account for random errors in the measurements.
(b) The variation in pump-induced pressure buildup led to fluctuations in both volume flow and net head.
(c) In this specific measurement:
    1. The net head, set to 30 meters ($\approx$3 bar), exhibits an uncertainty within the 2σ interval of approximately $\pm 0.15\%$.
    2. Concurrently, the volume flow experiences fluctuations around 0.268%.
(d) Consequently, the total uncertainty includes a systematic error of $\pm 0.315\%$ for the net head and $\pm 0.469\%$ for the volume flow.

4. Results

The results presented in this study maintain a constant net head of 30 m to observe variations in flow rate, pressure, and jet behavior among different needle types. Figure 9 illustrates the flow rate behavior for six needle types across various nozzle openings (10 mm, 16 mm, 22 mm, and 30 mm) in comparison to an uneroded normal needle $[N_0]$ (depicted by the black line). Notably, the normal needle $[N_0]$, possessing the largest area, exhibits the lowest flow rate, while needles with surface-reduced areas $[N_{1,2,3}]$ consistently demonstrate higher flow rates for all nozzle openings.

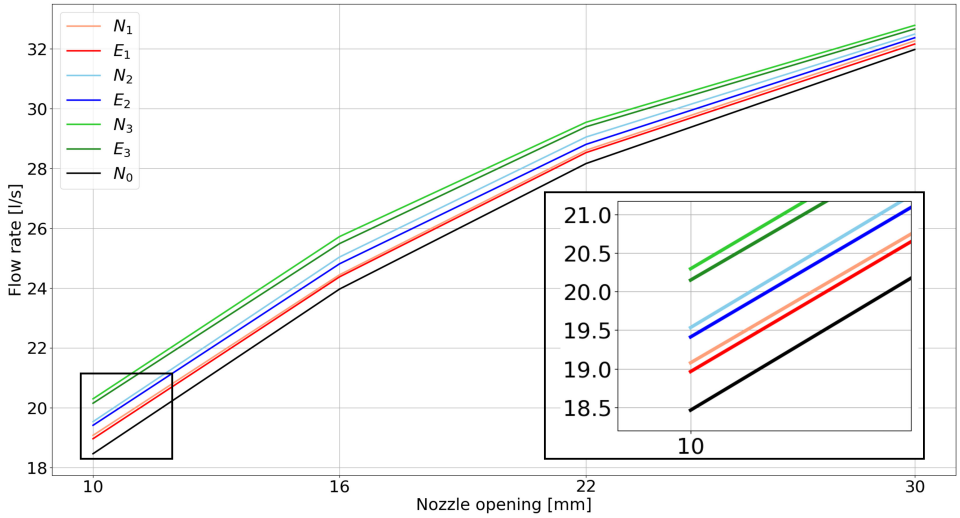

Figure 9: The Flow rate for Different Needles and Different Openings

The variation in flow rate due to an eroded surface $[E_{1,2,3}]$ was found to be smaller than the impact of the area-reduced needles $[N_{1,2,3}]$. Specifically, at a 10 mm opening, the variation between the normal needle $[N_0]$ and the 0.2 mm area-reduced needle $[N_2]$ demonstrates an increase in flow rate of approximately 5.8%. In contrast, the variation from $[N_2]$ to the corresponding eroded surface $[E_2]$ was found to be 0.6%.

This consistent difference in absolute flow rate between the area-reduced needle and the eroded needle holds for all openings. The close-to-parallel behavior of the flow rate for the two needles across different opening positions visually highlights this consistent relationship.

Examining the variation in flow rate, the data reveal a quadratic profile characterized by a positive and decreasing trend, regarding variations in the needle's opening position, area variation, and erosion depth. This behavior is illustrated in Figure 10. This trend transitions to a linear relation when the erosion depth component is excluded.

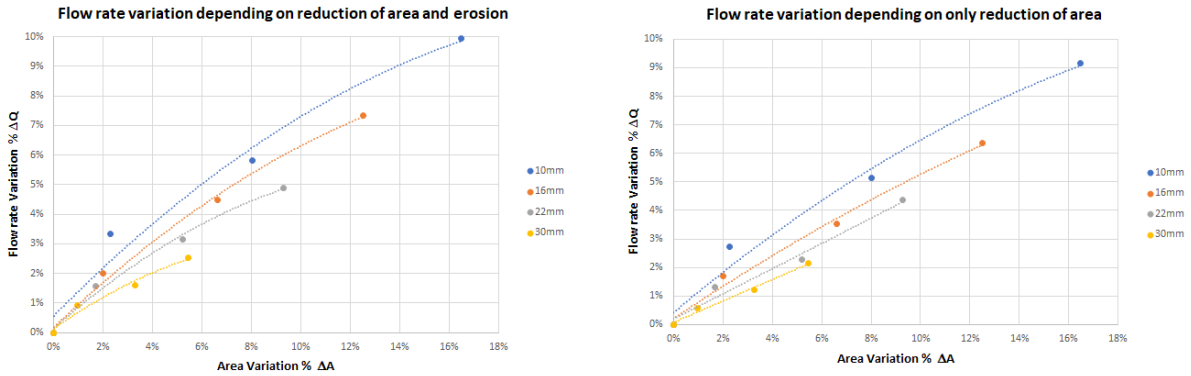

Figure 10: Left side shows the flow rate variation depending on variation of area and erosion depth. Right shown the flow rate variation only depending on the area variation

Regarding the impact of erosion on jet behavior, Figure 11 visualizes data obtained from edge detection on both sides in the horizontal plane of the jet. The left-hand side indicates the position of the needle relative to the seat ring at a 10 mm opening. Due to the camera position, the identification of the jet edge was not possible at the outlet of the nozzle and hence data is not available until a small distance downstream from the outlet. While this diagram provides a broader view of the analyzed jet area, the subsequent diagram offers a more detailed analysis of the area of interest due to slight jet diameter variations.

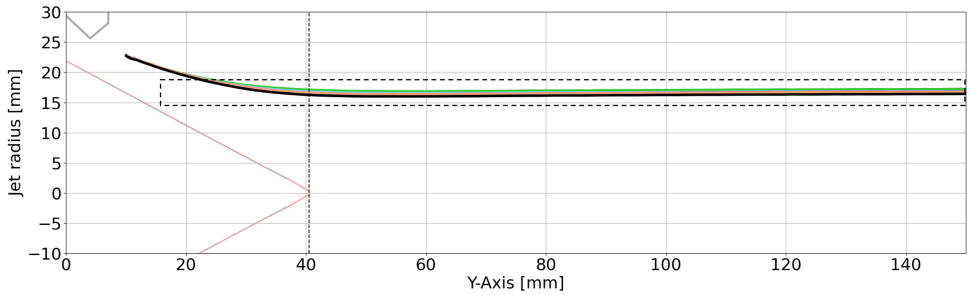

Figure 11: Overview of the detected jet edge through the image processing relative to the needle position

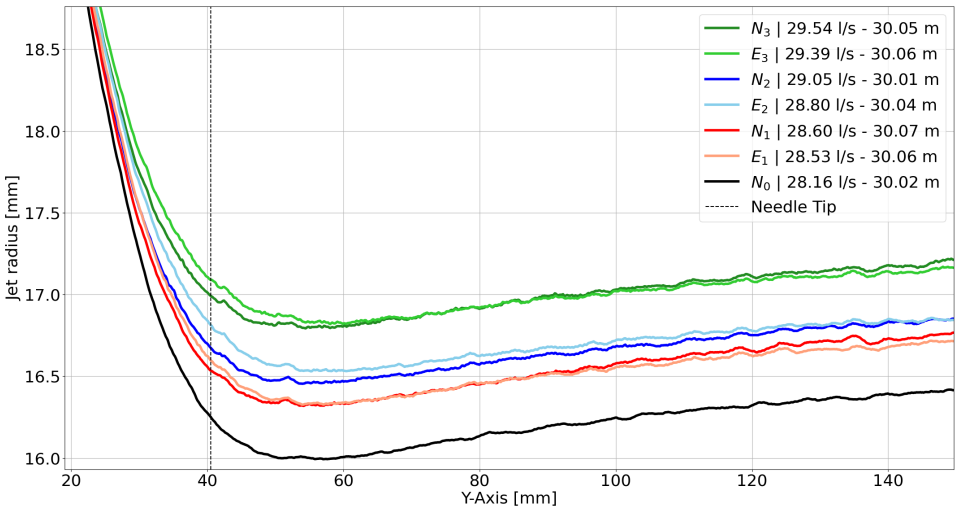

Figure 12: Variation of the jet radius between the surface reduced needle $[N_1, N_2, N_3]$ needles and the correlated eroded needles $[E_1, E_2, E_3]$ for a nozzle opening of 10 mm.

Figure 12 provides a detailed view where the dashed vertical line represents the needle tip, and the Y-axis represents the length downstream of the needle. The labels include the average net head and the average flow rate, both important in the influence on jet behavior and thus noteworthy. Observing the variation in flow rate reveals a clear trend: as the surface area of the needle decreases, the flow rate increases, resulting in a thicker jet diameter. Consequently, the normal needle $[N_0]$ exhibits the thinnest jet diameter, while the 0.3 mm reduced area $[N_3]$ demonstrates the highest diameter due to the increased flow rate resulting from the lower needle area. Additionally, an expansion in jet diameter along the flow direction is evident, primarily attributed to alterations in the flow profile within the jet which result in energy losses[9].

Concerning the comparison between the eroded needles $[E_{1,2,3}]$ and uneroded needles $[N_{1,2,3}]$ a noticeable observation is that the jet diameter of the eroded needle is found to be larger close to the nozzle outlet, despite having a lower flow rate. This phenomenon is further analyzed and visualized in Figure 13. This figure provides a detailed examination of the variation in the jet radius between needle pairs, focusing on the thickness variation.

The graph in Figure 13 illustrates the absolute difference between the area-reduced needles and their corresponding eroded counterpart. Notably, there is an increase in radius ranging from $0.2 - 0.3mm$, which manifests during the interaction between the jet and the needle surface. Following this initial jet radius increase, it gradually decreases for eroded needles, reaching a range of $0 - 0.1mm$ at approximately 11 cm downstream of the needle tip. A comparable trend is observed for a nozzle opening of 16 mm. However, for needle positions of 22 mm and 30 mm, this particular behavior is not recognizable anymore.

For a comprehensive assessment of jet edges, Figure 14 presents the variation of the right jet edge found from the image processing for the normal needle $[N_0]$ with a nozzle opening of 10 mm. The increase of surface roughness, due to erosion patterns, is influencing the topology of the jet [9]. It was also seen for all needles.

Upon examining plots of eroded needles, reduced area needles, and the normal needle, a noticeable trend emerges. The same fluctuation of the jet edge increases as expected along the flow direction. Initially, the jet radius fluctuation is less than 0.45%, but it progressively rises

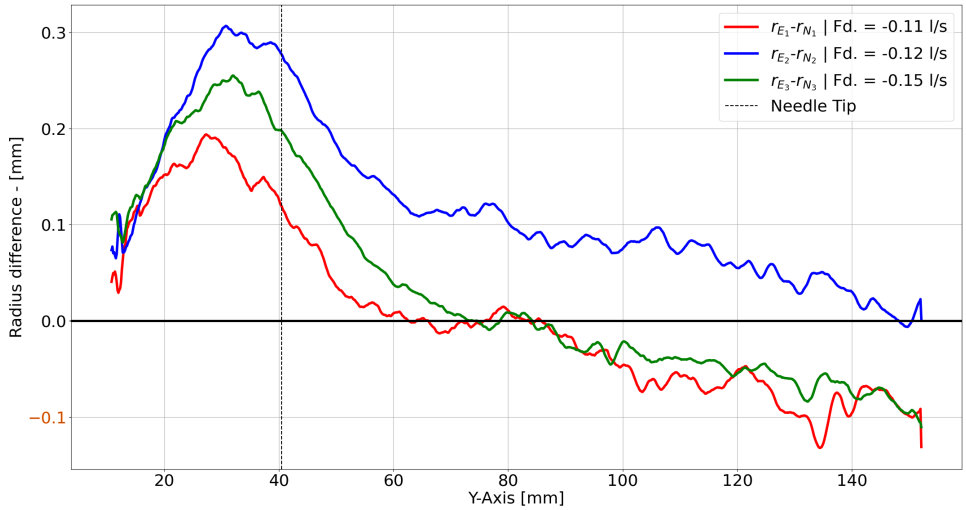

Figure 13: Relative radius difference between the eroded needle and its corresponding area reduced needle for a constant nozzle opening of 10 mm. In the label the "Fd." stands for "flowrate difference" between the eroded and uneroded one.

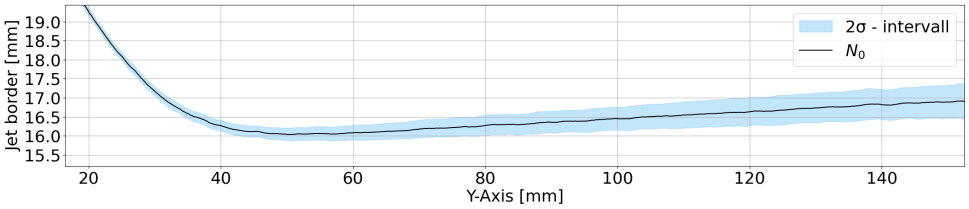

Figure 14: Variation of the jet border shown with of the 2 σ interval along the flow direction for a normal needle [N_0] with a 10 mm nozzle opening.

to about 3-3.5% after 14 cm further downstream. This consistent behavior in all the needles, suggests that there is no significant increase or decrease in the roughness of the jet radius due to erosion patterns or differences in needle area. It's important to note that due to system vibrations, there exists relative movement between the camera and the analyzed jet, introducing a constant error along the jet. This error must be smaller than the lowest detected standard deviation, in this case, less than 0,45%.

5. Discussion

The consistent variation in jet diameter while tiny nozzle openings due to erosion follow a recognizable pattern. Proximate to the needle area, there is a thicker diameter for the eroded surface, while a reduced or at least similar diameter is observed further downstream. This thickening effect along the needle's surface could be attributed to an increased boundary layer caused by erosion patterns, resulting in a reduction in average speed within this region. The subsequent decrease in velocity prompts an expansion in the cross-sectional area, maintaining the flow rate.

Furthermore, the flow rate for eroded needles consistently remains lower than that for uneroded ones, leading to a thinner diameter. This influence becomes more dominant further downstream, where the cross-section of the eroded needle jet becomes comparable to the average surface-reduced needles. To substantiate these hypotheses, CFD simulations involving different needle types could provide valuable insights into velocity profiles within the jet, contributing to

a deeper understanding of this phenomenon.

The increase in the boundary layer for eroded surfaces could also explain the lower flow rate observed in eroded needles across various nozzle openings. The constant net head of 30 meters ensures that the maximum jet velocity for all openings remains approximately the same at 24 m/s. A constant maximum velocity, as observed, might lead to a consistent boundary layer thickness for fixed erosion patterns, making it less correlated with the needle opening.

6. Conclusion

The findings presented in this paper offer a method to assess the impact of the erosion patterns on the flow rate and jet behavior. The results indicate that the average reduction in cross-section area due to erosion has a more significant effect on flow rate than the erosion patterns on the surface itself. Consequently, the lower cross-sectional area results in a more substantial increase in flow rate compared to the relatively minor decrease in flow rate due to erosion on the surface.

The high-speed camera analysis of the jet revealed an increase in jet diameter for decreasing the needle cross-section area leading to a higher flow rate. A secondary local increase in jet diameter was observed for tiny nozzle openings in the needle area due to erosion patterns. Despite a decrease in flow rate compared to the correlated area-reduced uneroded needle, the jet widened when erosions occurred on the surface.

The analysis of jet edge variation within the zone before reaching the runner, specifically the initial 14 cm in our test rig, yielded interesting insights. Although there was an expectation that the different stages of erosion evaluated could lead to a higher variation in jet edges and possibly result in droplet formation, no significant signs of an increase in the normal distribution of the jet were observed in this zone.

Acknowledges

The authors would like to acknowledge and thank the FME HydroCen - The Norwegian Center Research Center for Hydropower Tehcnology[10] for funding the project. In addition, ERASMUS must be acknowledged for their contribution in financing one of the authors stay at the Waterpower Lab at NTNU.

References

[1] Sangal S, Singhal M and Saini R 2018 *International Journal of Green Energy* **15** 1–22
[2] Thapa B 2004 *Sand Erosion in Hydraulic Machinery* Ph.D. thesis Norwegian University of Science and Technology, Faculty of Engineering and Technology
[3] Zidonis A, Petley S, Aggidis G, Benzon D, Panagiotopoulos A, Anagnostopoulos J and Papantonis D 2017
[4] Morris G and Fan J 1998 *Reservoir Sedimentation Handbook: Design and Management of Dams, Reservoirs, and Watersheds for Sustainable Use* McGraw-Hill books of interest (McGraw-Hill) ISBN 9780070433021
[5] A Karimi R S 1992 *Wear* **156** 33–47 ISSN 0043-1648
[6] Bajracharya T, Acharya B, Joshi C, Saini R and Dahlhaug O 2008 *Wear* **264** 177–184
[7] Solemslie B W and Dahlhaug O G 2019 *Tech. Rep. NEK IEC 60193:2019*
[8] Solemslie B W and Dahlhaug O G 2015 *Int. J. Hydropower Dams* **22** 78–83
[9] Staubli T, Abgottspon A, Weibel P, Bissel C, Parkinson E and Leduc J 2009
[10] URL `http://www.hydrocen.com/`

7. Appendix

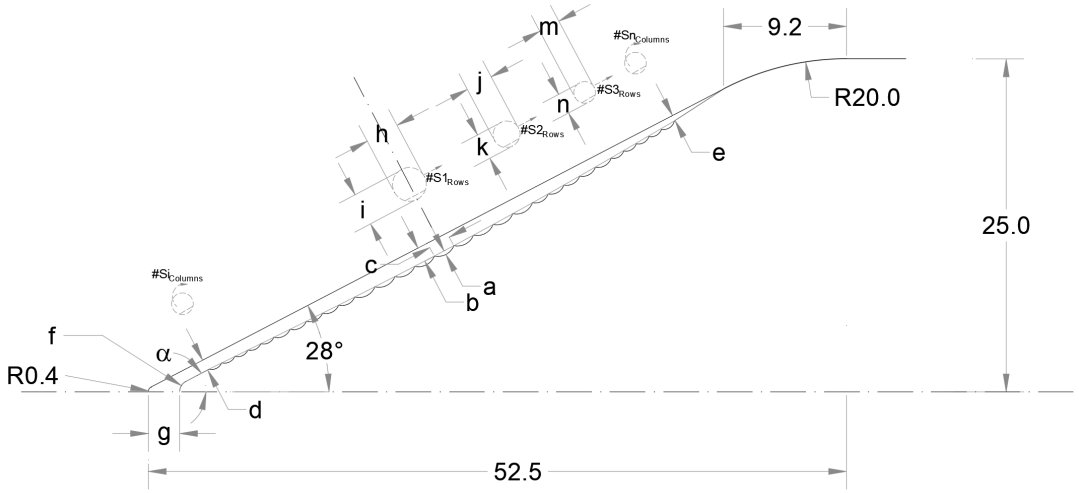

Figure 15: Main dimension for needles models.

Types	a	b	c	d	e	g	f	α	h	i	j	k	n	m	#S1 Rows	#S2 Rows	#S3 Rows	#Si Columns	#Si+1 Columns	#Sn Columns
N_0	-	-	-	-	-	-	-	-	-	-	-	-	-	-	-	-	-	-	-	-
N_1	-	0.2	-	0.2	0	0.8	R0.4	29.9°	-	-	-	-	-	-	-	-	-	-	-	-
E_1	0.1	0.2	1.0	0.2	0	0.8	R0.4	29.9°	2.4	2.1	1.9	1.7	1.6	1.3	7	8	10	20	Intrpl	250
N_2	-	0.6	-	0.6	0.3	1.5	R0.6	28.0°	-	-	-	-	-	-	-	-	-	-	-	-
E_2	0.2	0.6	1.3	0.6	0.3	1.5	R0.6	28.0°	2.3	2.3	1.8	1.8	1.5	1.5	6	7	7	30	Intrpl	250
N_3	-	1	-	0.8	0.4	2.4	R0.9	28.0°	-	-	-	-	-	-	-	-	-	-	-	-
E_3	0.3	1	1.7	0.8	0.4	2.4	R0.9	28.0°	2.5	2.5	2.0	2.0	1.6	1.6	5	5	5	40	Intrpl	300

Figure 16: Main dimension for needles models.

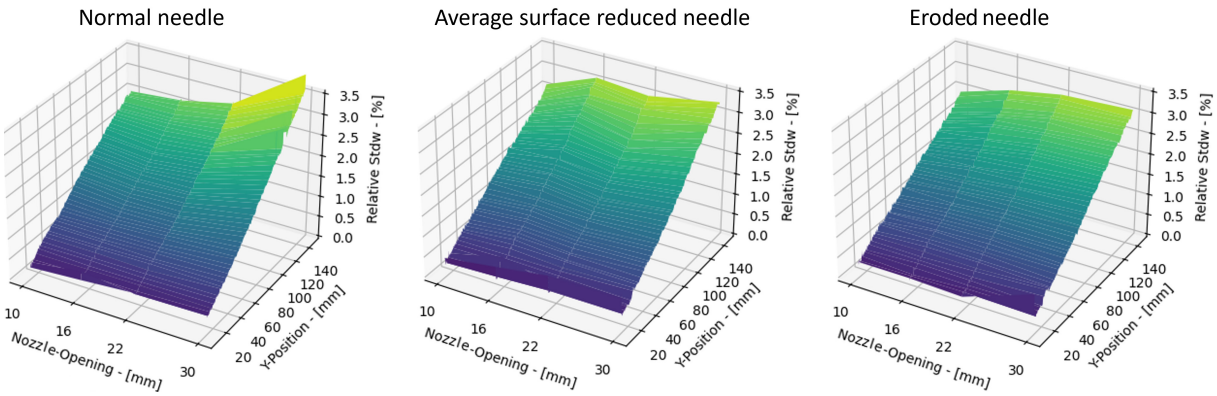

Figure 17: Relative variance of the jet edge relative to its diameter along the stream direction for the normal needle in comparison to the 0,3 mm surface reduced needle [N_3] and the corresponding needle with an eroded surface [E_3]. The Y-Axis shows the $2x\sigma$ normal distribution window.

Table 2: Average net head values for each examined experiment in [m]

Nozzle Opening	N_1	E_1	N_2	E_2	N_3	E_3
30 mm	30.06	29.97	30.03	30.02	29.97	30.04
22 mm	30.07	30.06	30.02	30.05	30.06	30.07
16 mm	30.09	30.02	30.03	29.95	30.03	29.98
10 mm	30.08	30.05	29.95	29.95	29.99	30.04

Table 3: Average Flowrate for each examined experiment in [l/s]

Nozzle Opening	N_1	E_1	N_2	E_2	N_3	E_3	
30 mm	32.27	32.16	32.49	32.37	32.79	32.67	31.98
22 mm	28.61	28.53	29.05	28.81	29.54	29.39	28.16
16 mm	24.44	24.38	25.04	24.81	25.72	25.49	23.97
10 mm	19.08	18.96	19.53	19.41	20.30	20.15	18.46

To investigate whether erosion significantly impacts secondary flows, the 3D plots in the appendix figure 17 illustrate the standard deviation increase relative to the jet diameter along the jet for the nozzle openings of 10, 16, 22, and 30 mm. These plots compare three needle types: needle [N_0], eroded needle [E_3], and reduced area needle [N_3].